The past, present, and future of x-ray technology for *in vivo* imaging of function and form

A. Fouras,[1,a)] M. J. Kitchen,[2] S. Dubsky,[1] R. A. Lewis,[3] S. B. Hooper,[4] and K. Hourigan[1]

[1]*Division of Biological Engineering, Monash University, Clayton, Victoria 3800, Australia and Fluids Laboratory for Aeronautical and Industrial Research, Monash University, Clayton, Victoria 3800, Australia*
[2]*School of Physics, Monash University, Clayton, Victoria 3800, Australia*
[3]*Monash Center for Synchrotron Science, Monash University, Clayton, Victoria 3800, Australia*
[4]*Department of Physiology, Monash University, Clayton, Victoria 3800, Australia*

Scientists and clinicians have a keen interest in studying not just the structure of physiological systems, but their motion also, or more generally their form and function. This paper focuses on the technologies that underpin *in vivo* measurements of form and function of the human body for both research and medical treatment. A concise literature review of x-ray imaging, ultrasonography, magnetic resonance imaging, radionuclide imaging, laser Doppler velocimetry, and particle image velocimetry is presented. Additionally, a more detailed review of *in vivo* x-ray imaging is presented. Finally, two techniques, which the authors believe are representative of the present and future of *in vivo* x-ray imaging techniques, are presented. © 2009 American Institute of Physics.
[DOI: 10.1063/1.3115643]

I. INTRODUCTION

Many of the most important processes in the human body have a mechanically dynamic component; that is, they involve motion. Obvious examples of this include the cardiovascular system, which involves the motion of the heart and the resultant flow of blood, the motion of the diaphragm and lungs and the resultant flow of air, and of course the motion of the musculoskeletal system. It follows directly from the vital importance of these mechanically dynamic systems that scientists and clinicians have a keen interest in studying not just the structure of physiological systems, but their motion also, or more generally their form and function. In many cases, the function of these systems relates to dynamic changes in the form over time, or motion and flow through these systems, or both. These measurements allow for a better understanding of the fundamental operation of the human body and serve as useful aids to the combat of dysfunction and disease of these systems.

Diseases of the vascular system remain the leading cause of mortality and morbidity in developed countries despite considerable therapeutic progress in recent years.[1–3] Thrombus formation can lead to various medical conditions including ischemia, atherosclerosis, and plaque rupture, the primary cause of stroke. Much progress has been made over the past 50 years in our understanding of the mechanisms involved in the formation of arterial stenoses. The importance of flow properties on the growth of atherosclerotic legions was first speculated in the late 1950s and early 1960s due to the observation that certain sites in the vasculature show a predilection to sclerotic growth.

It is now accepted that gradients in shear stress, both spatial and temporal, are the primary cause of atherogenesis.[2] Shear stress plays a vital role in platelet[4,5] and leukocyte[6] activation and adhesion. Furthermore, subtle shear stress changes have been shown to modulate thrombus formation and plaque rupture. A thorough understanding of the relationship between shear stress and atherosclerosis will aid developments in diagnosis and treatment of cardiovascular disease. It follows therefore that blood flow rate and velocity information has been reported to be critical for the diagnosis of vascular disease,[7–9] and methods to perform accurate and reliable assessment of instantaneous blood flow and velocity in a minimally or noninvasive manner have been researched extensively.[10]

Pulmonary disease, leading to respiratory failure, is one of the greatest causes of morbidity and mortality in humans. Chronic obstructive pulmonary disease, the fifth leading cause of death in humans, is currently present in 10% of the population and its incidence is increasing at a much greater rate than the other leading causes of death.[11] Similarly, respiratory failure is the greatest cause of morbidity and mortality in newborn infants, particularly those born very preterm, with many of the survivors (30%) developing bronchopulmonary dysplasia (BPD), which has significant implications for the respiratory health of the individual throughout the remainder of their life.[12] Our ability to reduce the burden of these diseases is greatly restricted by our inability to image the lung *in situ* with high resolution, particularly the small airways which harbor many of the pathologies associated with lung disease. Indeed, it is currently not possible to detect most forms of lung disease before it is clinically evident, making many of these diseases untreatable. However, a relatively common feature of many lung diseases (e.g., emphysema, pulmonary fibrosis, and BPD) is a regional alteration to the distal airway structure leading to marked regional changes in lung tissue compliance. Thus, imaging techniques that are capable of detecting regional differences in tissue velocities across the lung during the

a)Electronic mail: fouras@eng.monash.edu.

105, 102009-1

respiratory cycle are likely to detect the early stages of lung disease.

This paper focuses on the technologies that underpin *in vivo* measurements of form and function of the human body for both research and medical treatment. There exists a vast array of modalities that measure information regarding form and function. In particular, techniques which allow studies of the cardiovascular system and the lungs will be used as examples.

The most commonly used techniques to measure form have been x-ray imaging, ultrasonography, and magnetic resonance imaging. While these three modalities emerged as techniques to measure form, all three can measure both form and function. More recently, radionuclide imaging, laser Doppler velocimetry, and particle image velocimetry have emerged as techniques exclusively measure function.

These techniques will be discussed in a concise literature review and background section with which this paper begins. Next, the paper will focus on a review of technology of *in vivo* x-ray imaging. Finally, the paper proposes two techniques, which the authors believe are representative of the present and future of *in vivo* x-ray imaging techniques.

II. A CONCISE REVIEW OF TECHNOLOGY FOR *IN VIVO* IMAGING

A. Ultrasound

Ultrasound first appeared as an *in vivo* measurement tool in 1942. Ultrasonography uses ultrahigh frequency sound waves transmitted through and reflected by anatomical structures to produce images. The sound waves are created by piezoelectric crystals (the transducer) that change shape upon the application of an electrical potential difference. The transducer then becomes the detector in a reverse process by converting the reflected sound waves into measurable voltages. The most common form of modern ultrasound is known as B-mode ultrasound. In this mode, an image of the two-dimensional (2D) fan shaped region irradiated by the transducer can be constructed from the strength and return time of reflected signals received by the detector.

Velocity can be measured through use of Doppler or pulsed wave (PW) Doppler techniques. Doppler ultrasound utilizes the phase shift experienced by a continuous stream of vibration reflected from a moving object reported by Doppler in 1842. PW ultrasound measures relative changes in reflections between discrete packets of sound waves. Both techniques can only measure velocity on the axis of the ultrasound fan. Currently the gold standard technique for noninvasive *in vivo* measurement of flow velocity is duplex ultrasound. Duplex ultrasound is a combination of 2D ultrasound imaging and Doppler or PW velocity measurements. Color-flow duplex sonography (in which average blood velocity is color coded and superimposed on a gray scale image of structure measured by traditional ultrasonography) has become the most widely used noninvasive method for assessing vascular occlusive disease because it avoids the expense and risk of routine angiography.[13]

Although ultrasound imaging is inexpensive, portable, and widely available, this modality has a number of limitations. Ultrasound produces images that have low spatial resolution compared with those produced by imaging modalities such as magnetic resonance imaging or computed tomography (CT). The frequency of the sound waves ranges from 2 to 40 MHz. Today's electronics are capable of recording these signals in real time such that ultrasonography offers excellent temporal resolution. Unfortunately the spatial resolution is generally very poor, as is the penetration depth of the sound waves. The largest penetration depth is about 30 mm at frequencies near 2 MHz. At this depth the spatial resolution is typically around 0.7 mm. Using frequencies near 10 MHz the resolution can be improved to about 0.15 mm but the penetration depth reduces to little more than 6 mm.[14] Even the maximum resolution described here is around 15 times larger than an erythrocyte demonstrating that ultrasound is not capable of resolving blood flow with great detail. By using ultrasound at the limit of 40 MHz, a resolution of 40 μm is possible but clearly penetration will be limited to a few millimeters, most likely restricting suitability to small animal studies.[15] Furthermore ultrasound is known to have results highly dependent on operator skill[16,17] and requires acoustic access to the measurement region. This limits measurements through bone, gas, or deep layers of tissue. Lung tissue has therefore been categorized as unsuitable for clinical examinations with ultrasound.[18]

Interestingly it took quite a long time after the introduction of color flow imaging for the study of blood flow for the same technology to be applied for moving tissue. It is now recognized that the color-coding images of moving solid tissue are also of clinical utility.[17] The process, known as tissue Doppler imaging (TDI), is primarily used in cardiology and can be used to investigate motion of the myocardial wall during the cardiac cycle. TDI can be used to assist in the diagnosis of a number of conditions including coronary artery disease, hypertrophic cardiomyopathy, and arrhythmia.[19] With the presence of tissue wall velocity data, the tissue strain can be measured. However, dependency on image quality and subjectivity of the visual analysis remain major limitations.[19]

B. Laser Doppler velocimetry

Laser Doppler velocimetry (LDV) utilizes the Doppler effect to measure the velocity of tracer particles. When light is scattered off a moving particle, the frequency of the reflected light will be shifted proportionally to the velocity of the particle. When combined with a nonshifted reference beam, the interference pattern created can be directly related to the velocity of the scattering particle. LDV is inherently a point measurement technique. Full field flows can be measured using scanning techniques;[20] however, this decreases temporal resolution. Multiprobe approaches can help to overcome this limitation but temporal resolution is still not adequate to sample at a frequency sufficient for physiological heart rates. Serov *et al.*[21] applied LDV to full field skin perfusion measurements using an infrared laser. Light in the infrared spectrum has a maximum penetration of only a few millimeters in tissue, and hence this technique is limited to vasculature close to the skin surface.

C. Magnetic resonance Imaging

Magnetic resonance imaging (MRI) relies on the detection of radio frequency (rf) waves emitted by nuclei within an object as they relax from an excited energy state, having gained energy from an external rf pulse, to a more stable equilibrium state. The energy states are determined by a magnetic field used to align the precessing nuclear magnetic moments either parallel (lower energy) or antiparallel (higher energy) to the field. A specific rf must be applied to excite the nucleus into the quantized excited energy state. The MRI signal only arises from nuclei with unpaired nucleons which together yield a net magnetization in the applied field. Hydrogen atoms abound in biological materials and so ^{1}H MRI (sometimes called proton MRI) is commonly used for soft tissue imaging. The strength of the measured signal depends on the strength of the applied field. This means that very high field strengths, in the order of 1 T, are required for medical imaging.[14,22]

Among the most important applications in cardiovascular medicine are the diagnoses of heart failure, heart valve disease, and vascular disease. MRI is also the only *in vivo* modality capable of the quantification of leakage and obstruction of the heart valves, which is of great clinical importance.[23]

Velocity may be probed by MRI in various ways. The most accurate techniques are phase-shift or phase contrast velocity mapping.[24,25] In such measurements, a phase map of the MRI signal is drawn throughout space. Velocity information is obtained by comparing in each single voxel the measured phase with the zero phase of a flow-compensated reference phase map. Because detailed information about flow inside each voxel is available, phase-shift methods currently offer the best spatial resolution. They are also the most accurate and can measure displacements of less than 1 μm and velocities as small as 10 μm$\cdot$s^{-1}.[23]

The spatial resolution depends on the magnetic field homogeneity and gradient steepness as well as the bandwidth of the rf signals. In clinical settings the best resolution is around 0.5 mm, although this can be improved using high gradient field strengths. Because of signal-to-noise constraints, voxels usually cannot be much smaller than one-hundredth of the sample size. MRI scans typically require a few minutes to acquire data sets of relatively large objects (e.g., chest images) with good contrast. This results in a requirement for breath-holds and collection of data over multiple cycles for ensemble averaging.[26,27]

D. Radionuclide imaging

Nuclear medical imaging modalities utilize the detection of γ-ray photons emitted from within a patient by a pharmaceutical labeled with a radioactive isotope. The radio-labeled substance is used to preferentially target an organ or disease process. These methods are used for functional as opposed to anatomical studies. Although localization of the labeled pharmaceutical to specific areas can provide excellent contrast, nuclear medicine techniques generally suffer from poor signal-to-noise ratios as the amount of radioactive material must be minimized for patient safety.

There are three main modalities used in nuclear imaging. These are planar imaging, single photon emission computed tomography (SPECT), and positron emission tomography (PET). Planar imaging is a single projection method (like x radiography) where the emitted γ-rays are collimated and collected by a photon counting detector. SPECT is a tomographic version of planar imaging and works in a manner similar to x-ray CT by recording many projections in a ring about the patient, enabling image slices to be reconstructed for three-dimensional (3D) imaging. Unfortunately the spatial resolution of these systems is rarely better than 8 mm.[22] Low counting rates result in a single projection taking upward of 20 s to acquire, making the total acquisition time extremely slow unless a bank of detectors surrounding the patient is used.[14]

As its name suggests, PET is a tomographic technique that employs positron emitting radio nuclides. The positrons annihilate with electrons within the subject to produce two γ-ray photons traveling in opposite directions. By using a ring of coincidence detectors around the patient the photon pair can be determined and the position of the annihilation event can be estimated. This improves the spatial resolution over the SPECT technique to values approaching 3 mm. Recent improvements in detector technology have improved the spatial resolution for small animal imaging with microPET systems, with resolutions down to 2.3 mm.[28] Typical acquisition times for human PET imaging are of the order of tens of minutes to achieve reasonable statistics, although images acquired in tens of seconds can still show useful results for dynamic studies.[14]

For lung imaging, nuclear medicine enables studies of lung physiology and metabolism, including regional perfusion (gas exchange), water content, blood volume, enzyme and receptor studies, and gene expression.[29] While these are certainly useful applications, nuclear imaging is not ideal for studying lung anatomy or physiology due to the poor spatial and temporal resolution.

E. Particle image velocimetry

Particle image velocimetry (PIV) is well established within the field of fluid mechanics.[30] Importantly it has been shown to be capable of accurately measuring instantaneous velocity fields that have a high dynamic range.[31] In PIV, regions of fluid containing multiple tracer particles (typically illuminated by a visible wavelength laser) are imaged at two points in time, separated by a known time interval, and processed using correlation software. Figure 1 illustrates the standard PIV image processing procedure. The image pairs are discretized into interrogation regions. Cross correlation is performed between image pairs on each interrogation region and statistically, the maximum value of the cross correlation is the most likely particle displacement within the interrogation region.

PIV has many variations: stereo PIV where two (or more) cameras image from two different perspectives to measure three components of the velocity field,[32–34] holographic PIV where images of particles are acquired holographically allowing for three components of the velocity
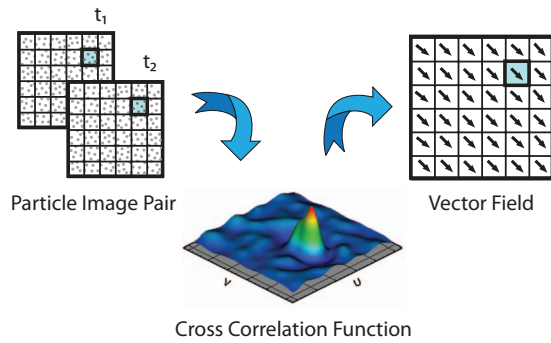
FIG. 1. (Color) Schematic diagram illustrating PIV image processing. The figure shows the discretization of image pairs, the calculation of cross correlations, and the resultant vector fields.

field over a 3D domain,[35,36] and even topographic PIV where the pressure field of a fluid flow can be inferred from PIV data acquired from a set of opposing cameras.[37,38] A review of the applications of PIV to medical research, demonstrating a number of such case studies, can be found in Ref. 39. The application of PIV to medical imaging is almost exclusively carried out through the use of the variant known as micro-PIV (μPIV).[40]

μPIV usually involves the illumination of the imaging region by a laser light fed through the microscope objective lens. It is also often used in conjunction with fluorescent particles and a dichroic filter to pass only fluoresced wavelengths in a system called epifluorescent microimaging. A schematic diagram of one implementation of such an imaging system is shown in Fig. 2. While this prevents the measurement of form, as only the fluorescent particles are imaged, it significantly increases signal-to-noise ratio for measurement of flow. The narrow depth of focus of the optical system is used to define the 2D measurement plane. Accuracy and spatial resolution are limited by signal-to-noise ratio and the diffraction limit of the optical system. Ensemble averaging of the correlation functions can be used to reduce the effect of noise for steady and periodic flows. Available spatial resolution is on the order of 1 μm.[41] Consideration must be given to out of focus particles, which will contribute to the correlation functions and may introduce a bias into the measurements.[42]

A major drawback of μPIV is the requirement of optical access, which limits its application *in vivo* to thin-walled,
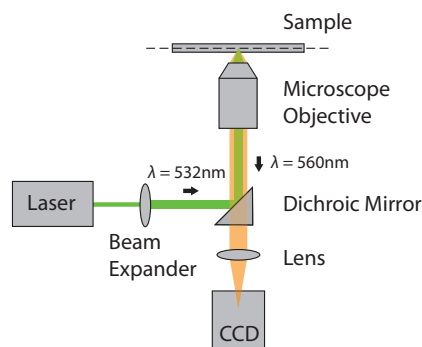
FIG. 2. (Color) Schematic diagram illustrating μPIV setup. The figure shows the epifluorescence imaging system that is typically used for measurement of exteriorized blood vessels.

externalized vessels. μPIV has been used to measure flow profiles in surgically exposed mesentery vessels of rats.[43,44] These studies used red blood cells as tracer particles. Vennemann *et al.*[45] measured two components of velocity within an embryonic avian heart using μPIV. Fluorescent particles were injected into live chicken embryos and the left ventricle was imaged using a fluorescence microscope. Measurements were taken at nine points on the cardiac cycle at a spatial resolution of 41 μm. PIV is clearly a highly effective technique with much to offer measurement of function; however, the requirement for optical access must first be overcome. Later in this paper a new version of PIV that utilizes x-ray illumination is discussed.

F. X-ray imaging

The first clinical x-ray images were taken in February 1896, not long after the discovery of x rays by Roentgen[46] in November 1895. As a consequence of the extremely small wavelength of x-ray light (subnanometer) x-ray imaging has an unequaled theoretical resolution and excellent ability to penetrate deep within tissue. X-ray imaging can be used to measure the form of the human body with the techniques of radiography for measuring 2D projections. Often a radio-opaque dye or contrast agent is used to enhance the contrast, as in techniques such as angiography and bronchography. Further enhancement can be achieved by a technique known either as bichromography or *K*-edge subtraction imaging. Radiographic projections can be combined to give a 3D tomographic reconstruction by a technique known as CT. X-ray imaging has been combined with the family of techniques known as video densitometry to measure the key function of vasculature blood flow.

For the reasons of penetration depth, resolution, and signal-to-noise ratio outlined here x-ray imaging is by far the dominant form of medical imaging today. Currently at least ten x-ray images are acquired for each of the other imaging modalities. Furthermore other improvements are made possible by the availability of extremely brilliant, coherent, and monochromatic x-ray radiation from synchrotron radiation sources. For this reason the authors will focus on x-ray imaging technology that offers both form and function for the remainder of this paper.

III. PAST TO PRESENT: A CONCISE REVIEW OF X-RAY TECHNOLOGY FOR *IN VIVO* IMAGING

A. Radiography

Despite the potential hazards of ionizing radiation, projection x radiography is one of the most frequently used imaging techniques. In fact, dental imagery depends almost entirely on x radiography and for mammography it remains the gold standard for early breast cancer detection.[22] Its relatively low cost, high spatial resolution, and ability to provide diagnostic information ensure its continued use.

Many advances have been made in x radiography since its advent. Significant improvements have been achieved in contrast due to the development of techniques for removing incoherently scattered x rays from the images. Spatial resolution has also improved with the advent of smaller and
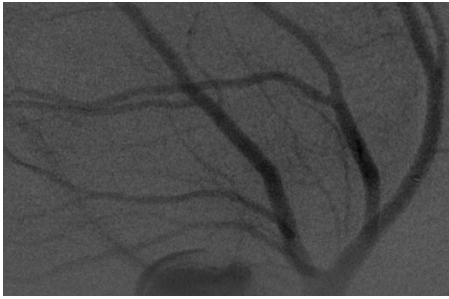
FIG. 3. A rapid contrast angiogram obtained from an adult rat. Recording was made using monochromatic x-ray radiation (SPring8, 33.2 keV) and a SATICON x-ray CCD camera system (pixel size of 8 μm) with a shutter open time of 2.5 ms under closed-chest conditions. The aortic root is clearly visible with the main branches of the left coronary artery. (Image courtesy of J. T. Pearson, M. Shirai, D. O. Schwenke, and K. Umetani.)

brighter focal spots. The greatest change in radiological practice in recent years came with the introduction of digital radiography, whereby radiographic images are digitized to enable radiologists to exploit the large dynamic range of x-ray attenuation images to improve their diagnostic capability.

In the 1990s came some of the first demonstrations that synchrotron radiation could be exploited to improve the quality of radiographic imaging. Using monochromatic, collimated synchrotron radiation to image mammography phantoms and excised breast tissue, it was shown that image contrast and spatial resolution were markedly improved over clinical mammography at a comparable or lower dose[47–50]). These results were not surprising since the beam hardening artifacts associated with the use of polychromatic x-ray sources have plagued x radiography since its inception. Moreover, the small source size and inherent collimation of synchrotron radiation ensure minimal penumbral blurring. Since these early experiments, synchrotrons have become an important research tool toward advancing radiography.

X rays are commonly utilized to observe specific structures and organs within the body through the use of contrast enhancing agents. Contrast agents are typically comprised of either a light weight material, such as air, or an electron dense medium, such as a radio-opaque dye to enhance absorption contrast. Examples include the use of air for imaging brain ventricles; barium compounds for the digestive tract; iodine compounds for examining kidneys, ureter tracts, blood vessels (angiography), and the coronary arteries (coronary angiography);[51] and xenon gas for studying the airways of the lungs (bronchography).[52,53] The utilization of contrast agents and the surgical procedures to introduce them have associated clinical risks, especially for the sick and elderly, with morbidity and mortality rates as high as 4% and 0.4%, respectively.[54,55]

An example of an x-ray angiogram can be seen in Fig. 3. This figure shows a rapid contrast angiogram obtained from an adult rat using iodinized contrast agent injected as a bolus into the aorta through a radiography catheter. Recordings were made using monochromatic x-ray radiation (SPring8, 33.2 keV) and a SATICON x-ray charge-coupled device (CCD) camera system (pixel size 8 μm) at 30 frames/s (shutter open time of 2.5 ms) under closed-chest conditions.

The aortic root is clearly visible with the main branches of the left coronary artery. (For further details of methodology and for an interesting example of quantitative functional measurements from angiography, see Ref. 56.) The image was enhanced by subtracting the background image (without contrast agent) from the raw version of the image shown (including contrast agent). This enhancement is a simple implementation of a technique known as digital subtraction angiography (DSA).

In DSA a baseline, or mask image (without the presence of contrast agent), is acquired and digitally subtracted from images of the same region in the presence of contrast agent. This gives striking images which show only the effect of the contrast agent without artifacts from the imaging system or tissue absorption. DSA systems are capable of displaying these enhanced images in real time. The obvious problem regarding such a subtraction is the alignment of detail on the mask and contrast images necessary due to motion of the imaging subject. A review of algorithms for reregistration of images can be found in Ref. 57. The use of DSA has grown to such an extent that in a clinical setting it is considered to be the standard angiography modality. In fact, Nederkoorn *et al.*[54] used DSA as the baseline for comparisons of Doppler ultrasound and MRI.

Contrast agent is normally injected into the arterial system, which can lead to complications including arterial blocking and excessive blood loss. In that situation surgical intervention becomes necessary,[58] and numerous patients have died in the process.[59] Intravenous injection is a safer alternative; however, by the time the contrast agent reaches the intended organ the concentration is so small that very high intensity, monochromatic radiation (e.g., synchrotron radiation) is required to observe sufficient contrast enhancement.[59] Another problem is the potentially toxic effect of contrast agents. Negative reactions to the various contrast media range from nausea and vomiting to seizures and cardiorespiratory arrest.[60]

B. X-ray videodensitometric flow measurement

As described above the use of angiography in a clinical and research setting has become commonplace. This means that both the procedures for injecting iodine and the necessary x-ray imaging equipment are ubiquitous throughout both the developing and the developed world. X-ray videodensitometric flow measurement is based on detection of the movement of radio-opaque contrast agent through the field of view. The first applications of videodensitometry date back to the 1950s.[10] These techniques involved the analog interrogation of x-ray film and subsequent analog analysis to measure flow. In modern times the use of digital detection systems and digital scanning of angiograms allows the use of digital computer analysis and implementations of relatively sophisticated and computationally expensive algorithms including the use of DSA. Shpylfoygel *et al.*[10] classified these techniques into bolus transport time algorithms, continuous velocity determination, contrast traversal distance algorithms, and droplet tracking algorithms.

These techniques reduce the angiogram to a profile (either spatial or temporal) of contrast agent density and use various measures to correlate the profile in either space or time. This analysis results in an estimate of either the time taken to travel a known distance or a distance traveled in a known time. The simplest of these involve the measure of distance traveled by the peak in bolus density between subsequent frames. Among the most complex of the techniques is the cross correlation of time-density curves. While there is no reference to the fact in the literature, this technique is very similar in concept to a much older technique used in light microscopy: dual slit cross correlation. Dual slit cross correlation was introduced by Wayland and Johnson[61] in analog form and in a more refined digital form by Zimmerhackl *et al.*[62] These techniques define two zones in a microimaging field of view and use cross correlation of intensity variations caused by the passage of erythrocytes to determine blood velocity.

Bogunovic and Loncaric[63] introduced a sophisticated technique which corrects for the 3D shape of the vasculature by combining CT data with the temporal angiography bolus transport time data. The CT data are used to create a 3D model of the vasculature, onto which the 2D angiograms are projected. This corrects for the potentially very large underestimation of velocity caused by the underestimation of vessel length that results from considering it to be 2D.

While these techniques can be considered minimally invasive the use of radio-opaque contrast agent does pose significant risks and can significantly alter the blood flow due to the method of injection or because of its significant viscosity relative to that of blood. Furthermore, all of these techniques result in a single measure of velocity, averaged across the entire vessel and over one or more cardiac cycles. This precludes any chance of measuring shear, which is perhaps emerging as the key indicator of a large number of pathologies and risks of pathology.[5,6]

C. Computed tomography

Computed tomography (CT) is an extension of x radiography that uses computer processing to convert a set of digital projection images, recorded from different perspectives in an angular space, into 2D and 3D data sets. This enables interior visualization of 3D structures from any perspective, or to observe single slices in cross section. A major drawback of conventional radiography is then overcome whereby objects overlapping in projection can obstruct the visibility of features of interest. The signal-to-noise ratio is increased over x radiography since the large number of projections increases the total measured signal, where the noise level is a fixed portion of the total intensity for photon counting statistics.[64]

The drawback to CT is that the large number of exposures results in a large dose compared to x radiography, approximately equal to the increase in the number of images recorded. For clinical CT systems over 300 images are typically recorded for a single 3D reconstruction. The patient dose in this process is around 8 mGy, which is roughly four

FIG. 4. CT image of a mouse upper torso with upper right quadrant of skull cut away to show nasal airways. (Image courtesy of K. K. W. Siu.)

times the average dose expected from annual background radiation. For this reason CT is not used for mass population screening.[22]

Spatial resolution for a given slice depends on the number of images acquired for each slice and the spatial resolution of each projection. This can be reduced by motion blurring. The spatial resolution can be as high as for conventional radiography, although high spatial resolution can lead to unacceptably high dose levels. The interslice spatial resolution depends on the method of image acquisition. If an area detector is used to record the projections then the resolution is set by the detector's resolution (plus penumbral blurring), whereas when imaging with one-dimensional detectors the slice resolution is determined by both the detector resolution and the translation distance of the object/detector between slices. For clinical systems a typical spatial resolution is of the order of 1 mm. This relatively poor resolution is imposed by dose restrictions. A 3D rendering of a CT of the upper torso of a mouse is presented in Fig. 4. In this figure, the upper right quadrant of the skull is cut away to reveal the internal detail of the nasal airways. Resolution is of the order of 10 μm. This CT is part of a functional study of the upper airways which is investigating the effects of cystic fibrosis and gene therapies for that disease.[65]

Temporal resolution can be a problem for CT since many projections must be acquired for the reconstruction. Today's rotating anode x-ray sources enable clinical chest scans to be recorded in tenths of a second; however, this time is increased when high spatial resolution is required.[22]

The great advantage of tomographic systems is their ability to provide volumetric information for anatomical or
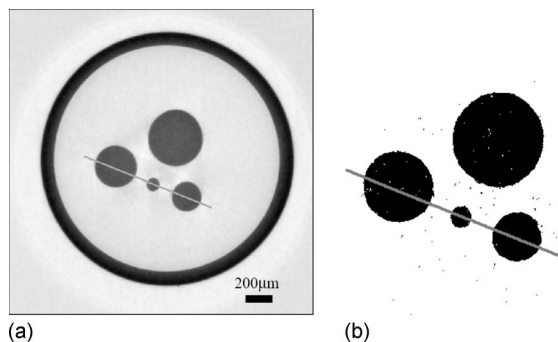
FIG. 5. Reconstructions of nylon phantom consisting of three nylon fibers inside an acrylic tube using (a) 720 projections and (b) limited projection binary algorithm of Ref. 66 with 20 projections. Note that the limited projection algorithm includes digital subtraction of outer Perspex tube. (Images courtesy of G. R. Myers.)

functional studies. For example, CT imaging of the lungs allows regions of tissue to be distinguished from air-filled regions by virtue of the density difference; this enables lung air volumes to be calculated with relative ease.[29] However, CT is not ideal for studies of physiological function since the temporal resolution is relatively poor when high contrast and spatial resolution are required.

The main drawbacks of CT stem from the large number of images required to reconstruct one CT data set. For the example of measuring lung volume listed above, the calculation of lung volume from CT and in many other cases a binary CT is sufficient and in these cases it is possible to perform reconstructions with many fewer projected images. Myers *et al.*[66] demonstrated excellent results with 5–20 projections. This results in a significant reduction in dose and in time required for a scan, also reducing motion artifacts and other complications arising from long scan times. An example from Myers *et al.*[66] is shown in Fig. 5. The figure shows a comparison of CT performed using the new limited projection algorithm with only 20 projections. The reduction in number of projections by a factor of 36 relates to an equivalent reduction in time and dose.

D. Synchrotron light source

It is well established that synchrotron radiation sources can produce x-ray beams in the diagnostic energy range (10–100 keV) that are many orders of magnitude brighter than conventional x-ray systems.[59,67] It is this brightness that enables the beam to be conditioned to increase the spatial and temporal coherence with sufficient flux remaining to record radiographic images at comparable time scales to conventional systems. Specifically, the beam energy spectrum can be filtered to a near-monochromatic condition to improve temporal coherence, while the source size can be reduced to enhance the spatial coherence. These types of beam conditioning create new possibilities for imaging that were not practicable with conventional x-ray sources.

Notwithstanding the dramatic advantages of the synchrotron light source, there is an accelerating development of new laboratory x-ray sources. These developments are aimed at making light sources which are small enough to fit into a laboratory or hospital and have fluxes that are comparable to those of third generation synchrotron sources. Recent examples of these developments can be found in Refs. 68–73. Tuohimaa *et al.*[72] described a microfocus source with dramatically higher flux[68,70,71,73] and described the development of ultrashort duration pulsed sources of very high brilliance. These ultrashort pulsed systems are of particular interest for dynamic measurements.

E. *K*-edge subtraction radiography (dichromography)

Monochromatic synchrotron radiation has enabled contrast enhanced x radiography to advance significantly due to a concept that was devised in the early 1950s.[67,74] This modality exploits the large change in x-ray absorption by elements at energies above and below their absorption edges. By acquiring two images above and below an absorption edge, the two images can be subtracted logarithmically to yield an image comprised of essentially just the contrast agent. Other structures obscuring the view of the agent-filled organ/vessel are effectively removed. This relies on the absorption of the remaining tissue not changing significantly between the chosen energy levels. Isolation of the tissue of interest dramatically increases the imaging sensitivity. This means that the contrast agent can instead be injected intravenously with relative safety, despite the fact that it is diluted during transit to the coronary arteries by approximately a factor of 50. Until now it has proved impossible to create x-ray beams which had both sufficient monochromaticity and sufficient flux for the technique to be useful.

To simultaneously achieve two monochromatic beams of different energies from a single polychromatic source requires a specially designed crystal monochromator. Various designs include the use of two misaligned and spatially staggered monochromator crystals[67,75] or using a single bent monochromator crystal.[59,67,76,77] In either case two spatially separated fan beams are created. The monochromator is designed such that the beams cross over at the patient and are therefore spatially coincident on the organ of interest. In order to construct a 2D image, the patient is scanned vertically through the two beams, and two single-dimensional line detectors are used to collect the transmitted radiation.

Although synchrotrons are not readily accessible to the general community, there are many cases where the comparatively safe dichromography, available only at synchrotron facilities, proves to be a useful technology. To date many hundreds of dichromography-type coronary angiograms have been successfully recorded for patients with heart disease at synchrotrons around the world.[59,78]

Another important application of synchrotron-based dichromography is bronchography, for which nonradioactive xenon gas mixed with oxygen is used as the inhaled contrast agent. This technique has been tested *in vivo*[67,79] and utilized for disease research using animal models at the European Synchrotron Research Facility.[52,53,80,81] In order to measure lung perfusion within the minor airways of animals, it is necessary to perform rapid tomographic reconstructions as the xenon is inhaled.

The success of the technique for measuring regional lung ventilation and the effects of broncho constriction in an

(a)   (b)
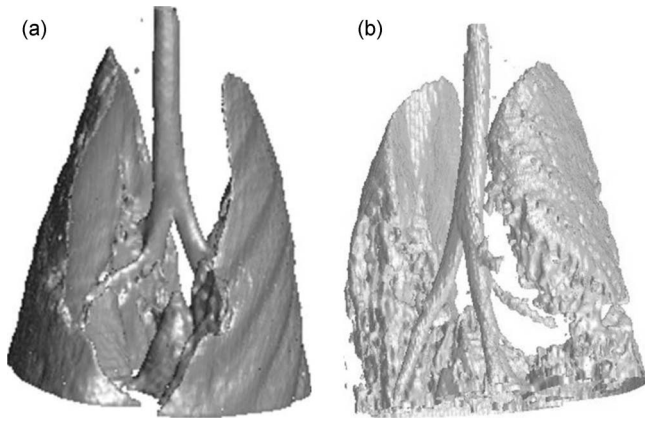
FIG. 6. Surface-rendered 3D lung images obtained in an adult rabbit at baseline (left) and at 8 min after histamine provocation (right). Images are obtained by *K*-edge subtraction imaging, which allows direct and quantitative measurement of the distribution of xenon gas inside the lungs. After histamine provocation, regional ventilation is reduced in some areas, and filling of the lungs is nonuniform (right). *(*Images courtesy of L. Porra.)

asthma model, induced via histamine provocation, are presented in Fig. 6. The left-hand image shows a *K*-edge subtraction CT reconstruction obtained in an adult rabbit at baseline (without histamine). The right-hand image shows the same lungs 8 min after histamine provocation. In the right-hand image, regional ventilation is visibly reduced in some areas and filling of the lungs is nonuniform.

F. Phase contrast x-ray imaging

By utilizing a partially coherent source of x rays, the wave nature of x-ray photons can be exploited to provide additional image contrast in x radiography. Changes imparted to the phase of an x-ray wave field by an object (a phenomenon commonly called refraction) can be rendered visible to produce "phase contrast" via interference with unperturbed waves or by introducing optical elements that selectively filter the perturbed wave field (see, for example, Ref. 82). Since the largest phase gradients occur at the boundaries between objects, phase contrast is predominantly an edge-enhancing effect. This can provide important diagnostic information by enhancing the visibility of tissue boundaries (see Fig. 7). For this reason the past decade has

FIG. 7. A conventional x-ray image (left, Faxitron) and a phase contrast x-ray image (right, SPring-8, 33 keV) of a (different) mouse nose region. Note the bright fringes around the sinuses (arrows) visible in the phase contrast image (right).

ushered in numerous advances in phase contrast imaging for biomedical applications using both laboratory-based and synchrotron radiation sources worldwide.

There are a number of implementations of phase contrast imaging, including crystal interferometry, grating interferometry, analyzer based imaging, and propagation-based phase contrast imaging (PBI).

Crystal interferometry can produce excellent measurements but requires a complex setup and typically requires the sample to sit within the interferometer. Yoneyama *et al.*[83] used a two crystal configuration to obviate this necessity. Grating interferometry is a much simpler technique that is a stronger candidate for clinical implementation. A recent example of grating interferometry can be found in Ref. 84. A common form of phase contrast imaging is analyzer based imaging. A number of differing implementations include Refs. 85–87 and recently Ref. 88.

These implementations of phase contrast imaging require complex configurations and when used for dynamic imaging these configurations must be very stable, with stability of the order of wavelengths for crystal interferometry. Additionally, these implementations are only capable of resolving one dimension of phase gradients, namely, those parallel to the plane of diffraction. Moreover, the use of additional optical elements invariably results in a significant reduction in flux, which can be critical for dynamic studies.

The simplest x-ray phase contrast technique is a form of Gabor's in-line holography[89] in which the coherent wave self-interferes upon propagation beyond the object.[90] This technique is often called PBI. This implementation has no requirement for complicated optics, with the exception of an optional monochromator, and this simplicity is well suited to dynamic imaging. PBI also measures two dimensions of the phase gradients providing a more complete image. The combination of these factors means that PBI is the most likely technique to succeed in a clinical setting. The contrast enhancement afforded by phase effects can be traded against a reduction in the x-ray dose delivered to the patient.

Phase contrast x-ray imaging (PCI) has not yet become a standard clinical imaging modality since its efficacy in medical imaging has yet to be fully established. However, the great potential for improving radiographic contrast has led numerous teams to explore the potential for PCI as a diagnostic tool for imaging blood vessels,[91] bone,[92] articular cartilage,[93,94] and other soft tissues.[95] When compared to conventional radiography, PCI is often capable of revealing structures that are otherwise invisible with x radiography. In conventional mammography, for example, breast tumors only appear visible due to slight differences in density to surrounding healthy tissues,[96] with a concomitant change in beam attenuation. Since phase visualization can improve image contrast, even between soft tissues, it has been shown that tumor detail can be more readily seen using PCI than with conventional radiography.[97–100]

A major emphasis is thus being placed on PCI as the next generation in mammography, with clinical trials already underway at the Italian synchrotron, ELETTRA.[100,101] The company Konica Minolta has already manufactured a laboratory-based phase contrast mammography unit. Trials
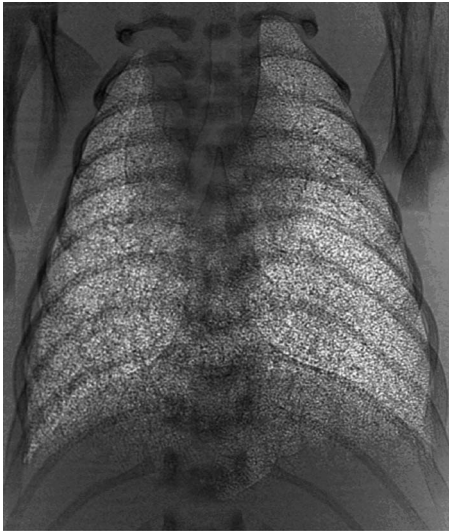
FIG. 8. Phase contrast image of deceased rabbit pup under artificial ventilation. Exposure time of 300 ms and energy of 25 keV. Ribs are visible as darker features, while the bright speckle pattern reveals the lung tissue.

with this system have already been reported using cancerous breast tissue samples.[69] These authors reported its superior ability at detecting breast mass and calcifications over a conventional system using the same exposure conditions. This study suggests that PCI could eventually become a common clinical imaging modality.

Diagnostic lung imaging also stands to benefit significantly from phase contrast imaging. The air/tissue interfaces provide the largest tissue density gradients within the mammalian body, which in turn provide the greatest x-ray phase gradients, making the lungs and other airways ideal for phase contrast imaging. For example, Westneat *et al.*[102] used dynamically recorded phase contrast image sequences to demonstrate that insect respiration is critically dependent on rapid tracheal compression in the head and thorax, a mechanism not previously understood.

Relatively few studies have focused on phase contrast imaging of the lungs since the complex lung structure produces patterns within the images that are difficult to interpret. With phase contrast, the lungs often appear decorated by a high contrast speckled pattern comprised of bright and dark dots having similar dimensions to alveoli.[95,103–106] An example of such an image can be seen in Fig. 8. It has been postulated that these speckles arise from focusing effects, whereby overlapping airways act as aberrated compound refractive lenses.[105]

The high lung contrast afforded by phase contrast imaging has been exploited to examine the clearance of fluid from the lungs of newborn rabbits.[107,108] These studies have investigated the rate and spatial pattern of lung aeration at birth with the aim toward assisting the ventilation of preterm infants, whose lungs have not developed sufficiently as a gas exchange organ. They found, *inter alia*, that body position plays an important role in lung aeration, whereby regions of the lung under highest gravitational pressure aerate slowest. Hooper *et al.*[108] also revealed that the transpulmonary pressures generated during breathing play a critical role in airway liquid clearance, a mechanism previously attributed to osmo-

sis arising from the active transport of Na^+ across the distal airway epithelium.

G. Phase retrieval

There is an ever increasing push toward quantitative imaging of form and function in medicine. Phase contrast not only offers improved image quality over conventional radiography, with an increased signal-to-noise ratio, but enables quantitative information to be extracted more accurately. In considering x rays as waves, an x-ray beam is completely described by its amplitude and phase. Although (phase) contrast can be gained by perturbing the phase of a partially coherent beam, only the intensity of the high frequency x rays can be recorded using current detector technology. In the equations describing the propagation of electromagnetic radiation through matter both the phase and absorption components are proportional to the material's atomic density (see, for example, Ref. 109). However, the phase term is typically three orders of magnitude greater than the amplitude term for biological materials at diagnostic x-ray energies (10–100 keV). Therefore, if the phase information can be recovered it can provide a more accurate measure of atomic density, particularly near the boundaries between tissues to which phase measurements are most sensitive. This additional sensitivity makes calculations of tissue properties, such as their projected thickness, appreciably more accurate.

The process of separating phase and attenuation information from intensity measurements is called phase retrieval. For all phase contrast modalities, phase retrieval involves measuring one or more images of the object after varying a parameter of the imaging system such as the object-to-detector distance or the x-ray energy. Phase retrieval can provide radiologists with both an attenuation image, of which they are intimately familiar, and a quantitative map of the tissue's phase properties, which is indicative of the tissue morphology (see also Refs. 88 and 109–111 and references therein). Radiologists can thus be armed with more information than is provided by conventional radiography.

H. X-ray particle tracking velocimetry

Recent publications have introduced x-ray particle tracking velocimetry (XPTV).[112,113] Seeger *et al.*[112] measured particle displacements in bubble columns using particle tracking. A medical biplane x-ray source was used to image the particles from orthogonal perspectives allowing three components of velocity to be reconstructed. The measurements were severely limited in spatial and temporal resolution due to limitations in the imaging equipment and the low seeding density necessary to resolve individual particles. Im *et al.*[113] used synchrotron x-ray imaging and particle tracking techniques to measure flow in a tube. This technique represents significant advances in both imaging and image processing over previous x-ray velocimetry publications. However, the velocity reconstruction method used is only applicable to axisymmetric flows in axisymmetric geometries. Furthermore all particle tracking techniques are limited by the dual requirement that particles can be individually identified in not one, but at least two imaging frames. In x-ray illuminated
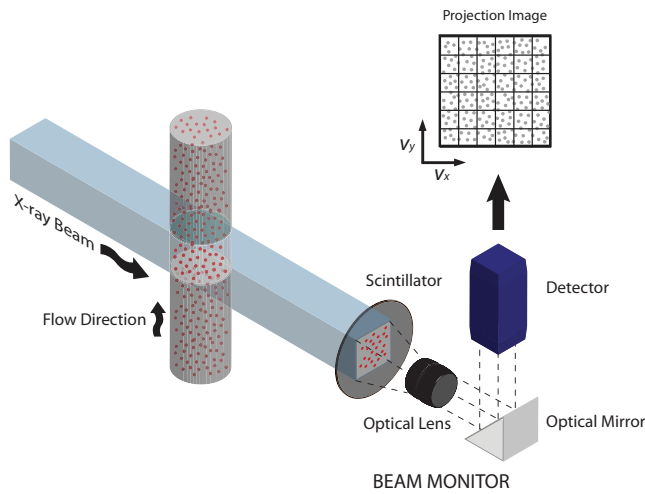
FIG. 9. (Color) Schematic diagram of x-ray illumination and imaging setup for x-ray PIV.

flows, where the velocity may vary through regions of 3D space that is mapped onto a single location in an image this becomes a highly complex and severely restricting limitation.

I. X-ray PIV

PIV is a newer flow measurement technique than PTV; however, it is well established within the field of fluid mechanics.[30,31] PIV has been shown to be capable of accurately measuring instantaneous velocity fields that have a high dynamic range. PIV differs from PTV mainly in that images are discretized and velocity measurements are performed statistically through the use of 2D cross-correlation functions. This significantly increases the robustness of the technique. There is no upper limit on tracers as there is no requirement to identify individual tracers in any sense and the addition of more tracers to images monotonically increases the signal-to-noise ratio. Furthermore, as a statistical measure, cross correlation is robust and not sensitive to noisy data.

PIV has been combined with x-ray imaging by at least two groups in recent years.[114,115] The penetrating power of x rays allows flow to be measured within opaque objects, with applications for noninvasive, high resolution blood flow field measurements. Figure 9 shows a schematic diagram of x-ray illumination and imaging setup for x-ray PIV. Kim and Lee[116] measured flow in tubes with particles[114] and blood

cells as tracers using x-ray PIV. The methods described in these studies are limited to two components of the average velocity within the measurement volume. These authors used traditional PIV algorithms designed for optical/laser based velocimetry. These algorithms assume pulsed (instantaneous) illumination and zero out-of-plane flow gradients and therefore fail to take into account the 3D characteristics of imaging real flows using x rays. This results in a significant underestimation of flow velocity. Fouras *et al.*[115] corrected this problem through the use of an algorithm that spans three frames rather than two and extrapolate the cross-correlation functions to the correct or ideal function. This results in a quantitative and high resolution measurement of velocity data.

The x-ray PIV analysis is taken one step further in Ref. 115. The paper showed that the correlation peak represents a probability density function (PDF) of the velocity within the measurement volume. When combined with certain assumptions about the flow field, it becomes possible to convert the volumetric PDF of the velocity to a velocity profile. This results in the capability to measure 3D flow data from single projection x-ray images.

An example of a reconstructed 3D velocity field, measured using x-ray PIV, is presented in Fig. 10. The figure shows the reconstructed flow inside a round pipe (color contours represent the velocity magnitude).[115]

IV. THE PRESENT AND FUTURE OF X-RAY TECHNOLOGY FOR *IN VIVO* IMAGING

Several examples of the latest technology for both the measurement of form and function are presented here. All examples provided have exploited the high flux, coherence, spatial resolution, and enhanced contrast offered by synchrotron-based phase contrast x-ray imaging. These case studies represent the cutting edge of the authors' research, and the results demonstrated are samples from techniques that are previously unpublished.

A. Computed tomographic x-ray PIV

Computed tomographic x-ray PIV (CTXPIV) is a technique under development which combines x-ray PIV, phase retrieval, and limited projection CT. It delivers three component velocity measurements for complex 3D flow fields, such as those found in the cardiovascular system.
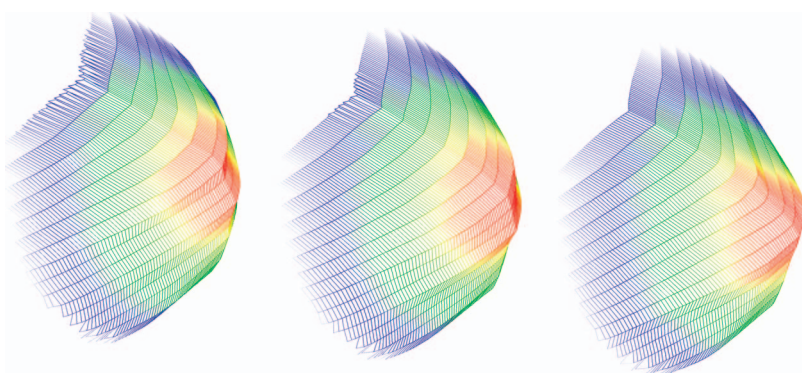
FIG. 10. (Color) Reconstructed 3D velocity field inside a round pipe measured using x-ray PIV. Color contours represent the velocity magnitude. From Ref. 115.

Single projection images are insufficient for evaluating three components of velocity. Images taken at a single projection angle contain no displacement information in the direction parallel to the x-ray beam. This limits single projection x-ray PIV to two component velocity measurements. In a method similar to CT, CT x-ray PIV overcomes this limitation by using multiple projection angles. Signal-to-noise ratios can be enhanced using phase contrast imaging and phase retrieval methods.[117]

As in single projection x-ray PIV, cross-correlation functions are calculated for interrogation regions within image pairs. The velocity field is reconstructed in axial slices, defined by the rows of interrogation regions for all projection angles. A three component, 2D, rectangular grid model represents the velocity field for each slice. Estimated cross-correlation functions are generated for every angle and every interrogation region within each slice. The estimated cross-correlation functions are generated using convolution of the measured autocorrelation function with the velocity PDF for the interrogation region within the model. The velocity coefficients in the model are iteratively optimized, minimizing the error between measured cross-correlation functions and the estimated cross-correlation functions, across all projection angles and interrogation regions simultaneously within that slice. Using this iterative approach, a model is reached which accurately represents the three component velocity field within each slice.

Figure 11 shows the reconstructed velocity field for a reversing flow (bottom) using only 19 projections. Synthetic particle images were generated using a reversing flow model (top). This first implementation of CTXPIV has accurately captured the flow structure, demonstrating the ability of CT x-ray PIV to measure nonaxisymmetric, 3D flow fields.

The small number of projections required is an important feature for reducing radiation dosage. It also allows the integration of CT x-ray PIV with a binary CT reconstruction, such as that described in the CT section above, delivering simultaneous measurement of both form and function.

B. Simultaneous measurement of lung structure, volume, and motion

Studies of lung aeration at birth are now advancing to investigate the distribution of ventilation at birth using mechanically ventilated prematurely born rabbit pups. The aim is to minimize ventilator-induced lung injury in preterm infants and identify the most appropriate strategies to aerate the lung. To that end we are developing novel algorithms to measure localized rates of lung aeration directly from the phase contrast images, as was first proposed by Kitchen *et al.*[118] We anticipate that by tracking the displacement of specific boundaries within the lung, using algorithms developed for PIV, that regional volume changes can be determined over areas approaching the dimensions of the terminal airways.

As the name implies, PIV is typically conducted with tracer particles used as a contrast agent that follows the flow of a gas or liquid. As discussed in the material relating to ultrasound, Doppler ultrasound can be used to measure not only the motion of blood in the heart but also the motion of
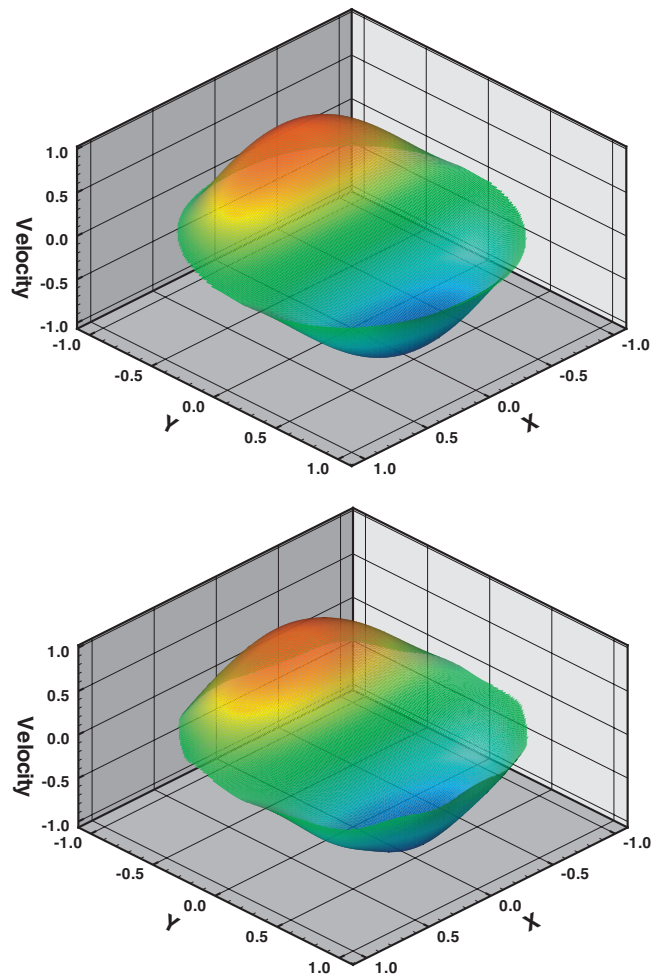
FIG. 11. (Color) 3D reversing velocity reconstruction using CTXPIV. Reversing velocity field used to generate synthetic particle images (top). CTXPIV velocity reconstruction using 19 projections (bottom).

the heart itself. In a similar way, PIV can be applied to the motion of tissue and organs. However, for PIV to be successful, a number of points (5–10) of detail or contrast are required for each velocity measurement. In the case of the lung, phase contrast produces a speckled intensity pattern which corresponds, in a complex way, to the airway morphology.[105] Tracking the motion of individual speckles can be used as an approximate means of tracking regional lung tissue displacement.

Figure 12 shows x-ray phase contrast images of a deceased pup ventilated by a small animal ventilator, similar to that in Fig. 8. The x-ray source was a monochromatic synchrotron beam at 25 keV. The detailed speckle pattern is clearly visible; the motion of which can be readily detected using PIV software. In Fig. 12 vector plots showing the motion of the rabbit pup lung between subsequent exposures are shown. Clearly visible during inspiration (left) is the pattern of expansion: both sides of the lungs appear to be expanding up against the chest wall and moving down into the diaphragm. During early stages of expiration (right) a simpler pattern of upward motion through the diaphragm is visible. These figures clearly demonstrate the simultaneous measure of form and function by a combination of PCI and x-ray PIV.
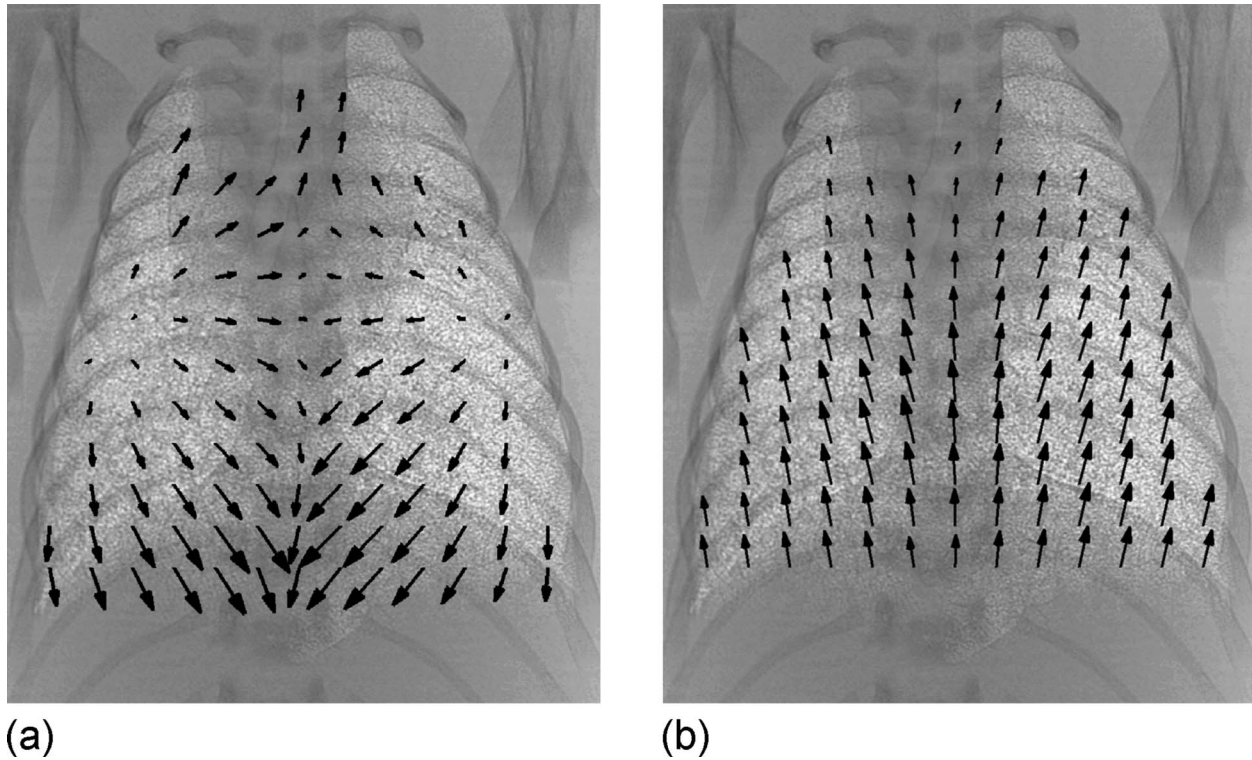
FIG. 12. Phase contrast images of rabbit pup lung under ventilation. Images acquired with 25 keV monochromatic synchrotron source. Superimposed on image are vectors showing lung velocity during inspiration (left) and expiration (right).

We have previously conjectured that the phase contrast speckle patterns of lung tissue, which relate to the complex structure of the lung, are likely to be altered by the progression of diseases that sufficiently alter airway morphology.[105] These changes may be detectable using data mining techniques or alternative image processing routines including phase retrieval. Moreover, we anticipate that exploitation of the PIV techniques may elucidate some of the characteristics of disease from phase contrast sequences of spontaneous breathing recorded *in vivo*.

V. CONCLUSIONS

There is an ongoing historical pattern of medical imaging technology reaching the milestone of measuring structure or form and later evolving to measure function. This can happen naturally as researchers apply the same technology that was once applied statically in a dynamic fashion or as new capabilities are added to that technology.

While there are a number of technology bases currently supporting *in vivo* measurement, three of these are dominant over all others: ultrasound, MRI, and x ray. Each has its own niche, and each, its own advantages and disadvantages. Ultrasound is ubiquitous largely because it is relatively inexpensive and can measure the key dimensions of form and function: structure and flow. Ultrasound is, however, limited by its wavelength in penetration and resolution and is highly dependent on the skill of the operator. MRI continues to improve and can readily measure multiple dimensions of form and function. However, MRI is limited in resolution both by the strength of the magnetic field and field gradients and by the signal-to-noise ratio. MRI can also be prohibi-

tively expensive and, as such, is not always available. X-ray imaging has the capacity to yield the highest resolution of all technology bases, is readily available throughout the world, and can penetrate all organ systems of the human body. The advent of the synchrotron light sources has opened up opportunities to measure both form and function through *k*-edge subtraction (KES), phase contrast imaging, x-ray PIV, and other modalities. Additionally, accelerating development of new less expensive (and hence potentially more readily available) x-ray sources may lead to the transfer of these technologies to the wider clinical and scientific communities.

Two case studies on techniques currently under development are presented: CTXPIV and the simultaneous measurement of lung structure, volume, and motion using phase contrast imaging. Both represent significant advances in the capability to measure both form and function. The development of these and other emerging technologies will not only depend on the technologies themselves but also on advances in supporting technologies such as x-ray detection. Furthermore, the authors believe that researcher should continuously progress in the dual efforts of developing the synchrotron imaging technology and seeking the means to transplant those technologies into the thousands of research laboratories and clinical centers lacking access to synchrotron radiation worldwide.

[1] E. Boersma, N. Mercado, D. Poldermans, M. Gardien, J. Vos, and M. L. Simoons, Lancet **361**, 847 (2003).

[2] S. A. Berger and L. D. Jou, Annu. Rev. Fluid Mech. **32**, 347 (2000).

[3] D. N. Ku, Annu. Rev. Fluid Mech. **29**, 399 (1997).

[4] W. S. Nesbitt, E. Westein, E. Tolouei, J. Fu, A. Carberry, J. Fouras, and S. P. Jackson, "Discovery of a new mechanism driving thrombus growth," Nat. Med. (in press).

[5] M. J. Maxwell, S. M. Dopheide, S. J. Turner, and S. P. Jackson, Arterioscler., Thromb., Vasc. Biol. **26**, 663 (2006).

[6] K. J. Woollard, D. Kling, S. Kulkarni, A. M. Dart, S. Jackson, and J. Chin-Dusting, Circ. Res. **98**, 149 (2006).

[7] H. Mast, J. Mohr, J. Thompson, A. Osipov, S. Trocio, S. Mayer, and W. Young, Stroke **26**, 1024 (1995).

[8] P. Turski, R. Levine, W. Turnipseed, and T. Kennell, Magn. Reson. Imaging Clin. N. Am. **3**, 541 (1995).

[9] S. Molloi, G. Bednarz, J. Tang, Y. Zhou, and T. Mathur, Int. J. Card. Imaging **14**, 137 (1998).

[10] S. D. Shpilfoygel, R. A. Close, D. J. Valentino, and G. R. Duckwiler, Med. Phys. **27**, 2008 (2000).

[11] R. A. Pauwels and K. F. Rabe, Lancet **364**, 613 (2004).

[12] J. J. Coalson, Semin. Neonatol. **8**, 73 (2003).

[13] C. A. Mistretta, J. Magn. Reson. Imaging **3**, 685 (1993).

[14] D. J. Dowsett, P. A. Kenny, and R. E. Johnston, *The Physics of Diagnostic Imaging* (Chapman and Hall, London, UK, 1998).

[15] A. Lyshchik, S. B. Hobbs, A. C. Fleischer, D. Khabele, D.-S. Son, J. C. Gore, and R. R. Price, J. Ultrasound Med. **26**, 1419 (2007).

[16] P. N. T. Wells, Phys. Med. Biol. **39**, 2113 (1994).

[17] P. N. T. Wells, Phys. Med. Biol. **51**, R83 (2006).

[18] P. C. Pedersen and H. S. Ozcan, Ultrasound Med. Biol. **12**, 483 (1986).

[19] G. Mundigler and M. Zehetgruber, J. Clinical Basic Cardiology **5**, 125 (2002).

[20] T. J. Essex and P. O. Byrne, J. Biomed. Eng. **13**, 189 (1991).

[21] A. Serov, B. Steinacher, and T. Lasser, Opt. Express **13**, 1681 (2005).

[22] C. Guy and D. Ffytche, revised ed., *An Introduction to the Principles of Medical Imaging* (Imperial College Press, London, UK, 2005).

[23] D. Bonn, S. Rodts, M. Groenink, S. Rafai, N. Shahidzadeh-Bonn, and P. Coussot, Annu. Rev. Fluid Mech. **40**, 209 (2008).

[24] C. L. Dumoulin, S. P. Souza, M. F. Walker, and W. Wagle, Magn. Reson. Med. **9**, 139 (1989).

[25] E. Fukushima, Annu. Rev. Fluid Mech. **31**, 95 (1999).

[26] H. B. Kim, J. R. Hertzberg, and R. Shandas, Exp. Fluids **36**, 455 (2004).

[27] F.V. Zananiri, Br. J. Radiol. **66**, 1128 (1993).

[28] D. J. Rowland, J. R. Garbow, R. Laforest, and A. Z. Snyder, Nucl. Med. Biol. **32**, 567 (2005).

[29] D. P. Schuster, A. Kovacs, J. Garbow, and D. Piwnica-Worms, Am. J. Respir. Cell Mol. Biol. **30**, 129 (2004).

[30] R. J. Adrian, Exp. Fluids **39**, 159 (2005).

[31] R. J. Adrian, Annu. Rev. Fluid Mech. **23**, 261 (1991).

[32] M. P. Arroyo and C. A. Greated, Meas. Sci. Technol. **2**, 1181 (1991).

[33] A. Fouras, J. Dusting, and K. Hourigan, Exp. Fluids **42**, 799 (2007).

[34] A. Fouras, D. Lo Jacono, and K. Hourigan, Exp. Fluids **44**, 317 (2008).

[35] J. Zhang, B. Tao, and J. Katz, Exp. Fluids **23**, 373 (1997).

[36] Y. Pu and H. Meng, Exp. Fluids **29**, 184 (2000).

[37] A. Fouras, K. Hourigan, M. Kawahashi, and H. Hirahawa, J. Visualization **9**, 49 (2006).

[38] A. Fouras, D. Lo Jacono, G. J. Sheard, and K. Hourigan, "Measurement of instantaneous velocity and surface topography of a cylinder at low Reynolds number," J. Fluids Struct. **24**, 1271 (2008).

[39] A. Fouras, J. Dusting, J. Sheridan, M. Kawahashi, H. Hirahara, and K. Hourigan, "Engineering imaging using particle image velocimetry to see physiology in a new light," Clin. Exp. Pharmacol. Physiol. **36**, 238 (2009).

[40] J. G. Santiago, S. T. Wereley, C. D. Meinhart, D. J. Beebe, and R. J. Adrian, Exp. Fluids **25**, 316 (1998).

[41] C. D. Meinhart, S. T. Wereley, and J. G. Santiago, Exp. Fluids **27**, 414 (1999).

[42] M. G. Olsen and R. J. Adrian, Exp. Fluids **29**, S166 (2000).

[43] K. Tsukada, H. Minimamitani, E. Sekizuka, and C. Oshio, Physiol. Meas. **21**, 459 (2000).

[44] Y. Sugii, S. Nishio, and K. Okomoto, Physiol. Meas. **23**, 403 (2002).

[45] P. Vennemann, K. T. Kiger, R. Lindken, B. C. W. Groenendijk, S. Stekelenburg-de Vos, T. L. M. ten Hagen, N. T. C. Ursem, R. E. Poelmann, J. Westerweek, and B. P. Hierck, J. Biomech. **39**, 1191 (2006).

[46] W. C. Röentgen, Nature (London) **53**, 274 (1896).

[47] E. Burattini, M. Gambaccini, M. Marziani, O. Rimondi, P. L. Indovina, M. Pocek, G. Simonetti, M. Benassi, C. Tirelli, and R. Passariello, Rev. Sci. Instrum. **63**, 638 (1992).

[48] E. Burattini, E. Cossu, C. Di Maggio, M. Gambaccini, P. L. Indovina, M. Marziani, M. Pocek, S. Simeoni, and G. Simonetti, Radiology **195**, 239 (1995).

[49] R. E. Johnston, D. Washburn, E. Pisano, W. C. Thomlinson, D. Chapman, N. F. Gmur, Z. Zhong, and D. Sayers, Proc. SPIE **2432**, 434 (1995).

[50] R. A. Lewis, K. D. Rogers, C. J. Hall, A. P. Hufton, S. Evans, R. Menk, G. Tromba, F. Arfelli, L. Rigon, A. Olivo, A. Evans, S. E. Pinder, E. Jacobs, I. O. Ellis, and D. R. Dance, in Medical Imaging 2002: Physics of Medical Imaging, San Diego, CA, 24–26 February 2002, edited by L. E. Antonuk and M. J. Yaffe [Proc. SPIE **4682**, 286 (2002)].

[51] S. H. Evans, in *The Physics of Medical Imaging*, Medical Science Series, edited by S. Webb (IOP, Bristol, UK, 1988).

[52] S. Bayat, G. Le Duc, L. Porra, G. Berruyer, C. Nemoz, S. Monfraix, S. Fiedler, W. Thomlinson, P. Suortti, C. G. Standerskjöld-Nordenstam, and A. R. A. Sovijärvi, Phys. Med. Biol. **46**, 3287 (2001).

[53] S. Monfraix, S. Bayat, L. Porra, G. Berruyer, C. Nemoz, W. Thomlinson, P. Suortti, and A. R. A. Sovijärvi, Phys. Med. Biol. **50**, 1 (2005).

[54] P. J. Nederkoorn, Y. van der Graaf, and M. Hunink, Stroke **34**, 1324 (2003).

[55] E. Cuddy, S. Robertson, S. Cross, and C. Isles, Lancet **366**, 1825 (2005).

[56] D. O. Schwenke, J. T. Pearson, K. Kangawa, K. Umetani, and M. Shirai, J. Appl. Physiol. **104**, 88 (2007).

[57] E. H. W. Meijering, W. J. Niessen, and M. A. Viegever, IEEE Trans. Med. Imaging **18**, 2 (1999).

[58] P. Armstrong, M. L. Wastie, and A. G. Rockall, *Diagnostic Imaging*, 5th ed. (Blackwell, Malden, MA, 2004).

[59] P. Suortti and W. Thomlinson, Phys. Med. Biol. **48**, R1 (2003).

[60] T. A. Farrell and M. L. Harvill, in *The Basics and Fundaments of Imaging*, 2nd ed., edited by W. E. Erkonen and W. L. Smith (Lippincott Williams & Wilkins, Philadelphia, PA, 2005).

[61] H. Wayland and P. C. Johnson, J. Appl. Physiol. **22**, 333 (1967).

[62] B. Zimmerhackl, J. L. Tinsman, and C. R. Robertson, Microvasc. Res. **30**, 63 (1985).

[63] H. Bogunovic and S. Loncaric, *MICCAI* (Springer-Verlag, Berlin, 2006), Vol. 4191, Pt. 2.

[64] J. T. Bushberg, J. A. Seibert, E. M. Leidholdt, Jr., and J. M. Boone, *The Essential Physics of Medical Imaging* (Williams and Wilkins, Baltimore, MD, 1994).

[65] D. W. Parsons, K. Morgan, M. Donnelley, A. Fouras, J. Crosbie, I. Williams, R. C. Boucher, K. Uesugi, N. Yagi, and K. K. W. Siu, "High resolution visualisation of airspace structures in intact mice via synchrotron phase contrast x-ray imaging (pcxi)," J. Anat. **213**, 217 (2008).

[66] G. R. Myers, D. M. Paganin, T. E. Gureyev, and S. C. Mayo, Opt. Express **16**, 908 (2008).

[67] R. Lewis, Phys. Med. Biol. **42**, 1213 (1997).

[68] H. Yamada, Nucl. Instrum. Methods Phys. Res. B **199**, 509 (2003).

[69] T. Tanaka, C. Honda, S. Matsuo, K. Noma, H. Oohara, N. Nitta, S. Ota, K. Tsuchiya, Y. Sakashita, A. Yamada, M. Yamasaki, A. Furukawa, M. Takahashi, and K. Murata, Invest. Radiol. **40**, 385 (2005).

[70] F. N. Beg, R. B. Stephens, H. W. Xu, D. Haas, S. Eddinger, G. Tynan, E. Shipton, B. DeBono, and K. Wagshal, Appl. Phys. Lett. **89**, 101502 (2006).

[71] L. M. Chen, M. Kando, J. Ma, H. Kotaki, Y. Fukuda, Y. Hayashi, I. Daito, T. Homma, K. Ogura, M. Mori, A. S. Pirozhkov, J. Koga, H. Daido, S. V. Bulanov, T. Kimura, T. Tajima, and Y. Kato, Appl. Phys. Lett. **90**, 211501 (2007).

[72] T. Tuohimaa, M. Otendal, and H. M. Hertz, Appl. Phys. Lett. **91**, 026102 (2007).

[73] H. Ikeura-Sekiguchi, R. Kuroda, M. Yasumoto, H. Toyokawa, M. Koike, K. Yamada, F. Sakai, K. Mori, K. Maruyama, H. Oka, and T. Kimata, Appl. Phys. Lett. **92**, 131107 (2008).

[74] B. Jacobson, Acta Radiol. (1921-1962) **39**, 437 (1953).

[75] G. G. Illing, J. Heuer, B. Reime, M. Lohmann, R. H. Menk, L. Schildwächeter, W.-R. Dix, and W. Graeff, Rev. Sci. Instrum. **66**, 1379 (1995).

[76] P. Suortti, W. Thomlinson, D. Chapman, N. Gm'ur, D. P. Siddons, and C. Schulze, Nucl. Instrum. Methods Phys. Res. A **336**, 304 (1993).

[77] H. Elleaume, A. M. Charvet, P. Berkvens, G. Berruyer, T. Brochard, Y. Dabin, M. C. Dominguez, A. Draperi, S. Fiedler, G. Goujon, G. Le Duc, M. Mattenet, C. Nemoz, M. Perez, M. Renier, C. Schulze, P. Spanne, P. Suortti, W. Thomlinson, F. Esteve, B. Bertrand, and J. F. Le Bas, Nucl. Instrum. Methods Phys. Res. A **428**, 513 (1999).

[78] B. Bertrand, F. Esteve, H. Elleaume, C. Nemoz, S. Fiedler, A. Bravin, G.

Berruyer, T. Brochard, M. Renier, J. Machecourt, W. Thomlinson, and J.-F. Le Bas, Eur. Heart J. **26**, 1284 (2005).

[79] J. C. Giacomini, H. Gordon, R. O'Neil, A. Van Kessel, B. Cason, D. Chapman, W. Lavendar, N. Gmür, R. Menk, W. Thomlinson, Z. Zhong, and E. Rubenstein, Nucl. Instrum. Methods Phys. Res. A **406**, 473 (1998).

[80] L. Porra, S. Monfraix, G. Berruyer, G. Le Duc, C. Nemoz, W. Thomlinson, P. Suortti, A. R. A. Sovijarvi, and S. Bayat, J. Appl. Physiol. **96**, 1899 (2004).

[81] S. Bayat, L. Porra, H. Suhonen, C. Nemoz, P. Suortti, and A. R. A. Sovijarvi, J. Appl. Physiol. **100**, 1964 (2006).

[82] R. Fitzgerald, Phys. Today **53**, 23 (2000).

[83] A. Yoneyama, N. Amino, M. Mori, M. Kudoh, T. Takeda, K. Hyodo, and Y. Hirai, Jpn. J. Appl. Phys., Part 1 **45**, 1864 (2006).

[84] M. Engelhardt, J. Baumann, M. Schuster, C. Kottler, F. Pfeiffer, O. Bunk, and C. David, Appl. Phys. Lett. **90**, 224101 (2007).

[85] E. Förster, K. Goetz, and P. Zaumseil, Krist. Tech. **15**, 937 (1980).

[86] T. J. Davis, D. Gao, T. E. Gureyev, A. W. Stevenson, and S. W. Wilkins, Nature (London) **373**, 595 (1995a).

[87] A. Bravin, J. Phys. D: Appl. Phys. **36**, A24 (2003).

[88] M. J. Kitchen, K. M. Pavlov, K. K. W. Siu, R. H. Menk, G. Tromba, and R. A. Lewis, Phys. Med. Biol. **52**, 4171 (2007).

[89] D. Gabor, Nature (London) **161**, 777 (1948).

[90] A. Snigirev, I. Snigireva, V. Kohn, S. Kuznetsov, and I. Schelokov, Rev. Sci. Instrum. **66**, 5486 (1995).

[91] V. N. Ingal and E. A. Beliaevskaya, Nuovo Cim. **19**, 553 (1997).

[92] K. Mori, N. Sekine, H. Sato, D. Shimao, H. Shiwaku, K. Hyodo, H. Sugiyama, M. Ando, K. Ohashi, M. Koyama, and Y. Nakajima, J. Synchrotron Radiat. **9**, 143 (2002).

[93] J. Mollenhauer, M. E. Aurich, Z. Zhong, C. Muehleman, A. A. Cole, M. Hasnah, O. Oltulu, and K. E. Kuettner, Osteoarthritis Cartilage **10**, 163 (2002).

[94] I. Koyama, A. Momose, J. Wu, T. T. Lwin, and T. Takeda, Jpn. J. Appl. Phys., Part 1 **44**, 8219 (2005).

[95] R. A. Lewis, C. J. Hall, A. P. Hufton, S. Evans, R. H. Menk, F. Arfelli, L. Rigon, G. Tromba, D. R. Dance, I. O. Ellis, A. Evans, E. Jacobs, S. E. Pinder, and K. D. Rogers, Br. J. Radiol. **76**, 301 (2003).

[96] P. C. Johns and M. J. Yaffe, Phys. Med. Biol. **32**, 675 (1987).

[97] C. J. Kotre and I. P. Birch, Phys. Med. Biol. **44**, 2853 (1999).

[98] E. Pisano, R. E. Johnston, D. Chapman, J. Geradts, M. V. Iacocca, C. A. Livasy, D. B. Washburn, D. E. Sayers, Z. Zhong, M. Z. Kiss, and W. C. Thomlinson, Radiology **214**, 895 (2000).

[99] F. Arfelli, V. Bonvicini, A. Bravin, G. Cantatore, E. Castelli, L. Dalla Palma, M. Di Michiel, M. Fabrizioli, R. Longo, R. H. Menk, A. Olivo, S. Pani, D. Pontoni, P. Poropat, M. Prest, A. Rashevsky, M. Ratti, L. Rigon, G. Tromba, A. Vacchi, E. Vallazza, and F. Zanconati, Radiology **215**, 286

[100] (2000).

A. Abrami, F. Arfelli, R. C. Barroso, A. Bergamaschi, F. Bille, P. Bregant, F. Brizzi, K. Casarin, E. Castelli, V. Chenda, L. Dalla Palma, D. Dreossi, C. Fava, R. Longo, L. Mancini, R.-H. Menk, F. Montanari, A. Olivo, S. Pani, A. Pillon, E. Quai, S. Ren Kaiser, L. Rigon, T. Rokvic, M. Tonutti, G. Tromba, A. Vascotto, C. Venanzi, F. Zanconati, A. Zanetti, and F. Zanini, Nucl. Instrum. Methods Phys. Res. A **548**, 221 (2005).

[101] F. Arfelli, A. Abrami, P. Bregant, V. Chenda, M. A. Cova, F. de Guarrini, D. Dreossi, R. Longo, R. H. Menk, E. Quai, T. Rokvic, M. Tonutti, G. Tromba, F. Zanconati, and E. Castelli, AIP Conf. Proc. **879**, 1895 (2007).

[102] M. W. Westneat, O. Betz, R. W. Blob, K. Fezzaa, W. J. Cooper, and W. K. Lee, Science **299**, 558 (2003).

[103] N. Yagi, Y. Suzuki, K. Umetani, Y. Kohmura, and K. Yamasaki, Med. Phys. **26**, 2190 (1999).

[104] Y. Suzuki, N. Yagi, and K. Uesugi, J. Synchrotron Radiat. **9**, 160 (2002).

[105] M. J. Kitchen, D. Paganin, R. A. Lewis, N. Yagi, K. Uesugi, and S. T. Mudie, Phys. Med. Biol. **49**, 4335 (2004).

[106] M. J. Kitchen, R. A. Lewis, N. Yagi, K. Uesugi, D. Paganin, S. B. Hooper, G. Adams, S. Jureczek, J. Singh, C. R. Christensen, A. P. Hufton, C. J. Hall, K. C. Cheung, and K. M. Pavlov, Br. J. Radiol. **78**, 1018 (2005).

[107] R. A. Lewis, N. Yagi, M. J. Kitchen, M. J. Morgan, D. Paganin, K. K. W. Siu, I. Williams, K. Uesugi, M. J. Wallace, C. J. Hall, J. Whitley, and S. B. Hooper, Phys. Med. Biol. **50**, 5031 (2005).

[108] S. B. Hooper, M. J. Kitchen, M. J. Wallace, N. Yagi, K. Uesugi, M. J. Morgan, C. Hall, K. K. W. Siu, I. M. Wliiams, M. Siew, S. C.Irvine, K. Pavlov, and R. A. Lewis, FASEB J. **21**, 3329 (2007).

[109] A. Momose, J. Synchrotron Radiat. **9**, 136 (2002).

[110] K. A. Nugent and D. Paganin, Phys. Rev. A **61**, 063614 (2000).

[111] T. E. Gureyev, T. J. Davis, A. Pogany, S. C. Mayo, and S. W. Wilkins, Appl. Opt. **43**, 2418 (2004).

[112] A. Seeger, K. Affeld, L. Goubergrits, U. Kertzscher, and E. Wellnhofer, Exp. Fluids **31**, 193 (2001).

[113] K. S. Im, K. Fezzaa, Y. J. Wang, X. Lui, and M. C. Lai, Appl. Phys. Lett. **90**, 091919 (2007).

[114] S.-J. Lee and G.-B. Kim, J. Appl. Phys. **94**, 3620 (2003).

[115] A. Fouras, J. Dusting, R. Lewis, and K. Hourigan, J. Appl. Phys. **102**, 064916 (2007).

[116] G. B. Kim and S. J. Lee, Exp. Fluids **41**, 195 (2006).

[117] S. C. Irvine, D. M. Paganin, S. Dubsky, R. A. Lewis, and A. Fouras, Appl. Phys. Lett. **93**, 153901 (2008).

[118] M. J. Kitchen, R. A. Lewis, S. B. Hooper, M. J. Wallace, K. K. W. Siu, I. Williams, S. C. Irvine, M. J. Morgan, D. M. Paganin, K. Pavlov, N. Yagi, K. Uesugi, and S. B. Hooper, Phys. Med. Biol. **53**, 6065 (2008).